JOURNAL OF GEOPHYSICAL RESEARCH, VOL. 104, NO. D2, PAGES 2131–2142, JANUARY 27, 1999

Lidar and numerical studies on the different evolution of vortex pair and secondary wake in young contrails

Ralf Sussmann
Fraunhofer-Institut fur Atmosphärische Umweltforschung, IFU, Garmisch-Partenkirchen, Germany

Klaus M. Gierens
Deutsches Zentrum für Luft und Raumfahrt, DLR, Wessling, Germany

Abstract. Vortex-regime evolution of contrails is investigated by focusing on the role of ambient humidity. Lidar cross-section measurements and observational analysis are combined with numerical simulations of fluid dynamics and microphysics. Contrail evolution behind four-turbofan aircraft is classified into three different scenarios. In the case of ice-subsaturated air, a visible pair of wingtip vortices is formed that disappears at the end of the vortex regime. In case of ice supersaturation, a diffuse secondary wake evolves above the wingtip vortices. It is due to detrainment of ice particles growing by sublimation of ambient humidity. A vertical wake-gap opens between the wingtip vortices and the secondary wake. It is due to subsaturated air moving upward along the outer edges of the sinking vortex tubes accumulating around the upper stagnation point of the vortex system. The vertical wake-gap preferably occurs in the wake of heavy (four turbofans) aircraft, since the vortices behind light aircraft migrate down too slowly. The secondary wake is composed of nonspherical particles larger than the ones in the wingtip vortices which are spherical particles and/or particles smaller than ≈ 0.5 μm. In most cases the secondary wake is the only part of a contrail that persists after vortex breakdown. This is because the ice in the vortex tubes evaporates due to adiabatic heating as the vortices travel downward. Only in the rare case of higher ambient ice supersaturation (>2%) do both parts of a contrail contribute to the persistent ice cloud. The number of ice crystals initially formed is typically reduced by a factor of 200 by evaporation (60% ambient humidity). This leads to a high population of interstitial particles. The results imply that formation of persistent contrails can be minimized by technical means.

1. Introduction

The most evident effect of air traffic upon the atmosphere is certainly its formation of (long living) condensation trails (contrails). These artificial clouds appear when the hot and humid exhaust gas from the jet engines reaches a water-supersaturated state during its mixing with the cold ambient air [*Appleman*, 1953; *Schumann*, 1996]. This then allows the water vapor to condense and freeze to form ice crystals. Ice clouds can also form in the wakes of airplanes by the dynamic perturbation of a highly ice-supersaturated environment [*Gierens and Ström*, 1998]. Contrails are generally believed to be persistent if the ambient atmosphere is at least ice saturated, although some evidence for persistence of contrails in subsaturated air has been found recently [*Sussmann*, 1997; *Sassen*, 1997]. Generally, persistent contrails receive more interest than those that are short living (lifetime <1 min), because only persistent contrails can significantly impact on the radiative energy balance of the Earth [*Ponater et al.*, 1996].

Understanding the mechanisms determining growth in the vertical and horizontal directions is crucial for quantifying the impact upon regional radiation balance. Vertical extension is ruled by the dynamics of the downward trailing vortex pair that forms behind cruising aircraft due to pressure differences at the wings ("vortex regime," ≈10–100 s behind aircraft). Horizontal growth is then determined by vertical shear of horizontal wind speed and turbulence in the "dispersion regime" [*Freudenthaler et al.*, 1995; *Gierens*, 1996; *Dürbeck and Gerz*, 1996]. This is after the breakdown of the trailing vortices which occurs typically 1.5–2 min behind aircraft.

Numerical simulations of the vortex regime have shown that the exhaust material behind each engine is entrained into the trailing vortices [*Quackenbush et al.*, 1993; *Miake-Lye et al.*, 1993]. Later, this material is partly detrained from the "primary wake," leaving back a vertical curtain of exhaust material ("secondary wake") above the downward traveling vortex pair. (Throughout this paper, "primary wake" means both the system of the two counterrotating wingtip vortices behind aircraft and the ice contained inside; "secondary wake" is the less ordered flow and ice above the primary wake). Hitherto, these processes were described in a number of theoretical investigations [*Scorer and Davenport*, 1970; *Gerz and Ehret*, 1996, 1997; *Schilling et al.*, 1996; *Spalart*, 1997]. In our preceding work we performed the first experimental study of the secondary-wake phenomenon and reevaluated the hitherto postulated mechanisms of vortex-wake entrainment and detrainment of fluid [*Sussmann*, this issue].

The main contribution to the ice mass of a persistent contrail has been assumed to be released from the vortices after the sudden vortex breakdown (i.e., vortex bursting and/or Crow instabilities [*Crow*, 1970; *Chevalier*, 1973; *Spalart and Wray*,

Paper number 1998JD200034.
0148-0227/99/1998JD200034$09.00

Figure 1. Photograph of a contrail in the transition between vortex and dispersion regimes around 1.5–3 min behind aircraft. On the left-hand side the vertical wake-gap is seen between the decaying primary wake and the diffuse secondary wake above. On the right-hand side the ice from the primary wake has evaporated, and only the secondary wake has become persistent.

1996]). Consequently, it was assumed that the maximum of the ice concentration and a cross-sectional bulge occurred in the lower part of the contrail. This was concluded from numerical studies simulating the behavior of passive tracers. However, we did not find this assumption to adequately describe the typical case for four-turbofan aircraft. Rather, from extensive observations of contrails during their late vortex phase and at the transition to the dispersion regime we found two characteristic phenomena which so far have not been described in the literature (Figure 1); i.e., (1) at some time during the vortex regime there appears a vertical separation of the contrail, i.e., a clearly visible "vertical wake-gap"; (2) at the transition to the dispersion regime, only the top part of the contrail remains persistent, while the separated bottom part disappears. This contradicts the above assumption that most of the ice particles in a persistent contrail originate from the primary wake (in the bottom part of the contrail) after vortex breakdown.

The goal of this paper is thus to understand the phenomena shown in Figure 1. In our preceding paper, dealing with entrainment and detrainment mechanisms, we conjectured the crucial role of ambient humidity in vortex-regime contrail growth. The investigation of the role of ambient humidity for contrail evolution during the vortex phase is thus the subject of the present paper. However, high-quality humidity measurements in the tropopause region are technically not available at present (although water-vapor differential-absorption lidar systems are becoming operational at this time). A further difficulty in this context is the high variability of ambient humidity. Changes in relative humidity by large factors are possible within horizontal scales of the order of 100 m. Hence, in addition to contrail analysis by lidar, we decided to perform the classical approach of statistical cloud observations as well as numerical simulations of fluid dynamics and microphysics where ambient humidity is treated as a free parameter. In

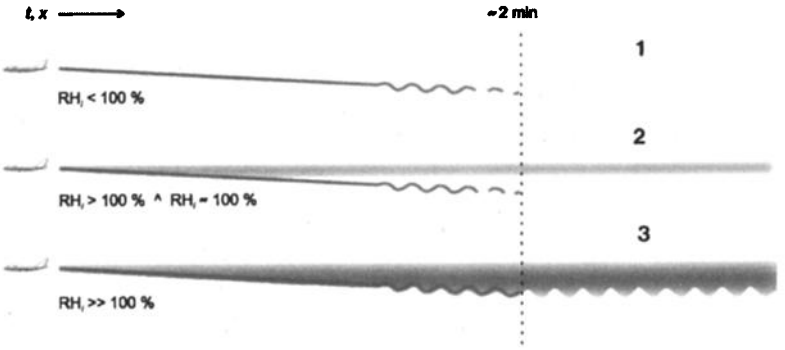

Figure 2. Three typical scenarios for the evolution of a contrail of four-turbofan wide-body aircraft from observational analysis, correlated with the natural cirrus frequency of occurrence: scenario 1, nearly no cirrus ($RH_i < 100\%$); 2, few cirrus ($RH_i > 100\% \wedge RH_i \approx 100\%$; "$\wedge$" means "at the same time"); 3, strong cirrus ($RH_i \gg 100\%$).

section 2 we first analyze extensive visual observations. We derive different typical scenarios of the cross-sectional evolution of a contrail from the vortex regime to the dispersion regime and correlate these scenarios with the actual coverage of natural cirrus. Subsequently, backscatter-depolarization-lidar measurements of both the vortex and the early dispersion regimes are discussed quantitatively. In section 3 we present numerical simulations that reproduce all of the cross-sectional scenarios found by observation. By this means we give insight to the physical mechanisms responsible for the details of the observed vortex-regime contrail evolution. The results are summarized, and conclusions are drawn in the final section 4.

2. Observational Results

2.1. Scenarios Related to Ambient Humidity

We obtained statistics on typical possible scenarios in the vortex-regime evolution of contrails from observing hundreds of aircraft at cruise conditions. In combination to each of the observations we investigated the occurrence of natural cirrus. This gives some (statistically valid) information on the ambient humidity levels in correlation to the observed scenarios. For all scenarios the Appleman threshold is fulfilled; the classification is as follows for four-turbofan aircraft (Figure 2).

2.1.1. Classification. The following scenarios were observed.

2.1.1.1. Scenario 1, about half of the observed cases: Visible contrails (vortex-wake pairs) are formed and remain visible up to the end of the vortex regime (age ≈1.5–2 min). No visible secondary wake is formed. All contrails of this scenario disappear completely at the end of the vortex regime marked by vortex breakdown. This scenario is observed typically when nearly no features of natural cirrus are present ($RH_i < 100\%$).

2.1.1.2. Scenario 2, about half of the observed cases (Plate 1): Visible vortex-wake pairs are formed which produce a secondary wake during the vortex regime. The secondary wake appears clearly separated vertically from the wingtip vortices during the late vortex regime (vertical wake-gap). Only the secondary wake remains persistent; that is, both wingtip vortices disappear suddenly after vortex breakdown. This scenario is observed typically for situations with few natural cirrus ($RH_i > 100\% \wedge RH_i \approx 100\%$, "$\wedge$" means "at the same time").

2.1.1.3. Scenario 3, rarely observable: In the remaining small (<5%) fraction of all four-engined aircraft contrails, there appears a continuous vertical curtain of ice particles from the wingtip vortices up to the flight level; that is, no vertical wake-gap appears. The whole contrail, including ice within the wingtip vortices, becomes persistent at the beginning of the dispersion regime. This is in most cases observed in combination with strong formation of natural cirrus; that is, $RH_i \gg 100\%$.

2.1.2. Discussion. The scenarios 1–3 reflect the fact that either no visible contrail is formed, a contrail that is visible up to 1.5–2 min is formed, or it becomes persistent for more than minutes up to hours. Any other scenario observed is not due to four-turbofan aircraft. Especially, the often observable short contrails, which evaporate after a few wing spans, are never due to heavy four-turbofan aircraft; they are due to light two-engined aircraft. Furthermore, the observations show that persistent contrails of four-engined aircraft only consist of the surviving secondary wake in the majority of all cases (scenario 2). The ice particles of the vortices suddenly evaporate in most cases at the end of the vortex regime, without leaving another diffuse cloud behind. This will be investigated by numerical simulations in section 3.

Obviously, the level of ambient humidity is a controlling factor for the formation of a secondary wake. We point out that a precondition for a secondary wake to be formed is that mechanisms leading to detrainment of fluid from the primary wake are active (due to baroclinic forces, shear, or turbulent erosion of the wingtip vortices). We concluded in our preceding paper that this precondition is usually fulfilled at cruising altitude [*Sussmann*, this issue].

We found that scenario 2, which needs slight ice supersaturation, is approximately as frequent as scenario 1, which occurs in subsaturated air. Cases with higher ice supersaturation, as required by scenario 3, are rare in our observations (only a few percent). The relative frequencies of these scenarios imply that situations with $RH_i > 100\% \wedge RH_i \approx 100\%$ are as frequent as situations with $0 \leq RH_i < 100\%$ in the upper troposphere; that is, the frequency distribution of RH_i should show a maximum at and slightly above 100%. The preference of the humidity for a value close to ice saturation (at least in case contrails are present) may be a general feature of the upper troposphere but may also be a result of the orographic influence of the Alps.

2.2. Lidar and CCD Camera Analysis

The instrumentation for ground-based remote sensing of contrails has been described in detail in our preceding paper

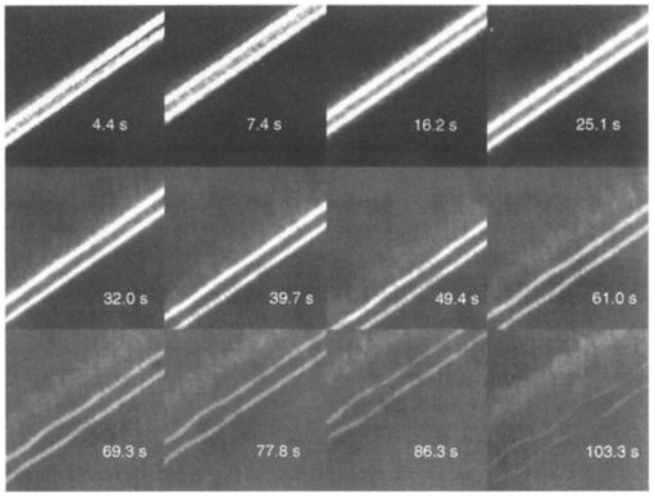

Figure 3. CCD image sequence of the vortex regime evolution of the contrail of a B-747. Detrainment of ice from the wingtip vortices leading to a diffuse secondary wake above starts as early as ≈4 s behind aircraft. The onset of the vertical wake-gap can be seen after 49.4 s.

[*Sussmann*, this issue]. Briefly, we use a backscatter-depolarization lidar at 532 nm (52 cm diameter Cassegrain telescope, Quanta-Ray GCR-4-10 laser). It is fixed on an angular scanning mount that can be computer controlled to track a contrail drifting with the wind. Cross-sectional backscatter images are obtained from stepwise angular scanning and recording of lidar profiles (10 laser pulses each). Cross-sectional images are obtained by graphical interpolation of lidar data. Parallel to the laser axis, a CCD camera is installed (Sony XC-77CE). It is utilized for documentation of the lidar scan and for determining wind speed and the speed of aircraft, as well as for stepwise imaging of contrail evolution.

2.2.1. Vertical wake-gap. In Figure 3 a CCD image series of the vortex-regime contrail of a B-747 aircraft is displayed. The sequence of images between 4.4 and 39.7 s behind aircraft shows the development of a diffuse secondary wake above the pair of wingtip vortices. We had already shown in our preceding work that the secondary wake onset starts as early as ≈4 s behind the aircraft [*Sussmann*, this issue]. We found that this corresponds to a stage where the jets of the inner engines are rolled a three-quarter period around the corresponding jets of the outer engines (Figure 9 of our preceding work). The onset of the secondary wake is thus due to an early detrainment of fluid. It originates essentially from the jets of the inner engines at the beginning. An increasing contribution of the outer engines is expected later.

The vortex tubes are seen to become continuously thinner during the vortex regime. This is both due to detrainment of ice particles from the vortices and to evaporation of ice particles within the vortices as a result of a growing saturation deficit during the downward migration (section 3).

Figure 3 shows the onset of the vertical wake-gap between the high-density pair of wingtip vortices and the diffuse secondary wake above after 49.4 s. The extension of this vertical wake-gap increases continuously till the end of our video image series at 103.3 s behind aircraft. The mechanism for the formation of the vertical wake-gap will be detailed by our numerical simulations of fluid dynamics and microphysics in section 3.

2.2.2. Vortex regime cross section. In Plate 1 the lidar-derived cross-sectional image of the backscatter signal of a vortex-regime contrail is displayed. This is ~50 s behind a B-747-400 aircraft, as has been discussed in detail in our preceding work [*Sussmann*, this issue]. Below, it will be discussed in comparison with a later-stage image at 2.8 min behind aircraft (see section 2.2.3).

Briefly, Plate 1 shows a vortex separation of 47 m and a vertical extension of 160 m. A diffuse triangularly shaped secondary wake is seen above the primary wake; a vertical wake-gap appears between primary wake and secondary wake. The cross-sectional area of the primary wake is 4620 m^2; the secondary wake encloses 4410 m^2 (cross section defined by the contour of a backscatter signal of 0.1; see Plate 1). We derived a ratio of 5:1 for the ice surface area within the primary wake relative to the ice surface area within the secondary wake after 50 s [*Sussmann*, this issue].

In our preceding work we investigated the lidar-derived linear depolarization ratio to obtain information on the particle sizes and shapes at 50 s behind aircraft [*Sussmann*, this issue]. Depolarization values around 0.35 within the primary wake indicated particles being small compared to the (523 nm) lidar wavelength and/or spherical particles. In the secondary-wake domain, depolarization values were around 0.5 as typically found for natural cirrus, indicating larger and hexagonal crystals.

According to its cross-sectional properties this lidar image (Plate 1) represents an example of scenario 2; see section 2. From this we conclude that ambient humidity had been $RH_i > 100\% \wedge RH_i \approx 100\%$ ("$\wedge$" means "at the same time"). We compare the findings of this section with numerical simulations performed for varied ambient humidity levels in section 3.

2.2.3. Early dispersion regime cross section. In Plate 2 the lidar-derived cross-sectional image of an early dispersion regime contrail is displayed (2.8 min behind aircraft). It shows a significant maximum of the backscatter signal in the upper part and a continuous decrease in cross-sectional width toward the lower edge. We found these phenomena to be typical for early dispersion regime cross sections. We give the following explanation for this special shape. It fits our above scenario 2; see section 2.1 and Figure 1 (right-hand side); that is, the backscatter signal only originates from the secondary wake that has become persistent, while the wingtip vortices are no longer visible. This becomes evident from comparing Plate 2 with the secondary wake shown in Plate 1. Also, there is a continuous narrowing of the cross-sectional width of the secondary wake toward the lower part. At 2.8 min behind aircraft (i.e., after vortex breakdown) the ice from the primary wake has already evaporated (see dashed circles in Plate 2 for an approximate location of the vortices before breakdown). We explain this by the relative humidity within the vortices becoming subsaturated by adiabatic compression during the downward vortex migration, as reflected by our numerical simulations (section 3).

The prominent maximum in the top part of Plate 2 could also have been assumed to be due to ice being released after bursting of the vortices located in the top part of the plate. This can be excluded, since in this case the vertical extension of 150 m would have to be attributed to a sedimentation of ice particles. To rule this out, we assume maximum terminal fall velocities of ice particles of 0.7 m/s [*Pruppacher and Klett*, 1997] and a fall time of at most 1.3 min. (Release of ice from vortex breakdown assumed not earlier than 1.5 min behind aircraft.)

By this we obtain a maximum vertical extension of 55 m at 2.8 min behind aircraft. The measured vertical extension of 150 m thus cannot be attributed to a fallout of ice particles. Furthermore, in numerical simulations of persistent contrails, sedimentation was not found to a considerable degree before an age of 0.5 hours since crystal diameters are still too small (~1 μm) [*Gierens*, 1996].

Knowing that the observed vertical extension is due to secondary-wake formation, the disappearance of the ice from the two wingtip vortices (dashed circles in Plate 2) has to be investigated. In particular, this finding is in contrast to recent numerical simulations that yield the maximum of ice concentration and a cross-sectional bulge after vortex breakdown in the lower part of the contrail. This discrepancy with the observational results is probably due to the fact that these simulations were restricted to passive tracers. In the following, we will present numerical studies, including microphysics, to obtain a simulation of the observed details of contrail evolution.

3. Numerical Simulations

3.1. Model Setup and Initialization

The simulations were performed with the hydrodynamics code MESOSCOP [*Schumann et al.*, 1987] which we have coupled with a spectrally resolving cloud microphysics model. The latter has been developed at the NASA Ames Research Center [*Jensen et al.*, 1994]. With these coupled codes we have simulated the evolution of contrails during the vortex regime, i.e., an early stage of contrail evolution (~10–100 s plume age). For details of these codes the reader is referred to the cited references.

The velocity field that constitutes the initial vortex pair of a wide-body four-turbofan aircraft has been provided by F. Garnier (personal communication, 1997) [see also *Garnier et al.*, 1997]. It is the vortex pair of a B-747 cruising at 10 km altitude with a speed of 250 m/s. The assumed weight of the aircraft is 285.4 tons. The computed circulation of each vortex is 540 m^2/s. Also, the initial temperature and tracer concentration fields have been computed by these authors, although their tracer concentration refers only to the exhaust from the two inner engines of the B-747. The corresponding distribution of the exhaust from the two outer jets has been estimated by ourselves. This was done such that the particles from the outer engines have a greater concentration around the vortex core than those from the inner engines. This is corroborated by the lidar-derived exctinction profile across the vortex center measured 23.1 s behind aircraft, showing a strong maximum at the vortex cores (Figure 1 of our preceding paper). The outer engines are closer to the wing tips from where the vortices originate. Thus the exhaust from the outer engines is more strongly attracted by the vortex cores than that from the inner ones; hence it is more concentrated. All the initial fields correspond to a plume age of 21 s.

For the present study we assume that ice crystals are the only class of particles present (i.e., no ambient aerosols, no liquid droplets). We use 25 logarithmically arranged bins to represent the crystal size spectrum, ranging from 0.1 to 25 μm. The crystal size doubles each three bins; the crystal mass doubles from one bin to the next. The only microphysical process considered in this study is condensational growth of ice crystals or the inverse process, i.e., evaporation (including complete disappearance of a crystal). Other processes, like coagulation, sedimentation, etc., are not important for ice crystals during a contrail's jet and vortex regimes [*Gierens*, 1996; *Chlond*, 1998]. Nucleation of new crystals on ambient haze particles that get close to the vortex system probably occurs [*Gierens and Ström*, 1998], but it is also ignored here, since we consider only cases with ambient humidity near ice saturation, where nucleation of new crystals would proceed at an extremely slow rate [see *DeMott et al.*, 1994, Figure 2].

The microphysical fields are initialized as follows: Inside the vortex pair we assume ice saturation. The total water content in this region (vapor and ice) consists of the background humidity that is partly entrained into the plume and partly sucked through the engines, plus the water vapor formed by the combustion of kerosene. For the latter, we assume an emission index of EI_{H_2O} = 1.24 kg/kg fuel, which yields 13.6 g water vapor from fuel combustion per meter of flight path in the plume. All the moisture above ice saturation is assumed to form the ice crystal population in the plume. We assume that there are 10^{13} ice crystals per meter of flight path in the initial plume (i.e., at 21 s plume age) which corresponds to an emission index for nonvolatile particles of about 10^{15} particles per kg fuel [*Petzold et al.*, 1997; *Kärcher et al.*, 1998; *Anderson et al.*, 1998]. Both ice crystals (number density) and the vapor from fuel combustion are distributed according to the concentration fields provided by F. Garnier (personal communication, 1997) and supplemented by ourselves (see above), which results in a smooth initial vapor concentration field. Hence the ice mass distribution inside the vortices is smooth initially. The ice crystals are distributed over the 25 bins such that a lognormal (mass) distribution with a geometric standard deviation of 1.92 results. The spectral details of the ice crystal size distribution are not important for the physical mechanisms we are going to investigate here. Hence they are not addressed in the present paper. Instead, we will only use the quantities crystal number density and ice water content.

A 2-D domain of 400 m × 800 m (cross section × altitude) is used for the simulations. The altitude range is 9,500–10,300 m, the contrail is formed at 10,170 m altitude. Vertical profiles of temperature and wind speed are obtained from measurements onboard the DLR research aircraft FALCON which were taken on a flight on April 22, 1996, over southern Germany. These data were recorded close to the lidar measurement (Plate 1) in time and space. For most of the simulations (including the reference case) the wind is ignored, and a smoothed temperature profile with a roughly constant lapse rate of 8 K/km is used. The temperature at flight altitude is −53°C. The ambient relative humidity (with respect to water) is treated as a free parameter and taken to be constant in the model domain. Atmospheric or aircraft-induced turbulence has been ignored for the sake of simplicity. The spatial resolution is 4 m, and the time step is 0.15 s. The time step must be that short because of the high swirling velocities in the vortices. The simulations end at 150 s simulation time (i.e., 171 s plume age) at latest. This is already a stage (the so-called dispersion regime) when vortex breakdown, due to Crow instabilities or vortex bursting has occurred [*Crow*, 1970; *Chevalier*, 1973; *Spalart and Wray*, 1996]. These effects, being three-dimensional, cannot be observed in the present 2-D simulations. Our look onto the late phases of the simulations should therefore not be too critical. In the following, one reference case plus five sensitivity cases are considered.

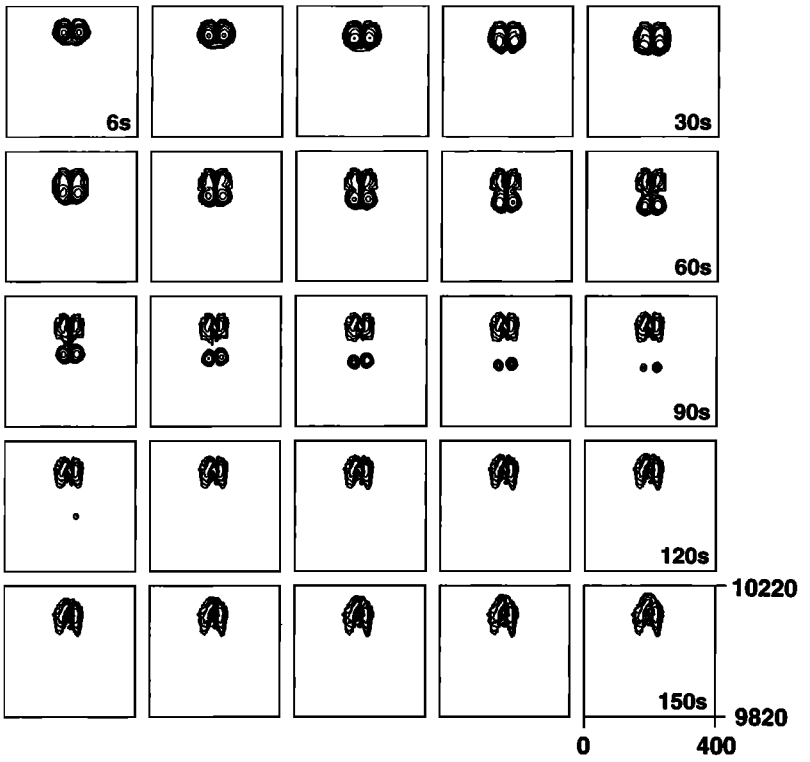

Figure 4. Time series of the simulated cross section of a contrail in scenario 2; that is, the ambient relative humidity is slightly exceeding ice saturation in the altitude of contrail formation. The contours show lines of equal ice water content, beginning with 10^{-2} g/m^3 (outermost contour) and increasing with steps of $10^{1/2}$. Each frame is 400 × 400 m^2 in size, the altitude range is 9820–10220 m. The frames follow each other in time steps of 6 s. Note that only the secondary wake forms the persistent contrail, whereas the ice in the downwelling vortex tubes evaporates.

3.2. Reference Case

Our reference case is characterized by a relative humidity with respect to liquid water of RH_w = 60%. In flight altitude this means a small ice supersaturation of about 0.8%, whereas beneath 10,050 m the air is subsaturated with respect to ice. The initial plume contains 14.2 g/m ice, which consists of 10^{13} crystals per meter with maximum number densities exceeding 10,000 cm^{-3}. The corresponding vapor content is 119 g/m.

3.2.1. Simulating the vertical wake-gap. Figure 4 shows the evolution of a young contrail in this environment. Displayed are (logarithmically spaced) contours of the ice water content (IWC). From the beginning the downward traveling of the vortex pair can be seen together with a simultaneous formation of the secondary wake. At least from the eighth frame on (i.e., at 48 s simulation time or 69 s plume age) a beginning detachment of the secondary wake from the vortex pair can be observed as a waist in the IWC contours. The separation is completed at 72 s simulation time (hereinafter written as "ST"). Thereafter, the vortex pair travels farther down, getting weaker and weaker until it disappears eventually. In turn, the secondary wake stays at rest at its initial altitude, and it will be persistent because of ice supersaturation at these altitudes. Obviously, this simulation reproduces what was labeled in section 2 as scenario 2.

A closer look at the fields of velocity and ice supersaturation (SI = RH_i − 100%), as well as to the distribution of IWC, reveals the physical mechanism that leads to the vertical wake-gap between the vortex system and the secondary wake. These fields are shown in Plate 3 for a ST of 66 s. The air inside the vortex pair is subsaturated, whereas at the same altitude, there is supersaturation in the environment. A maximum saturation deficit of more than 10% occurs close to the lower stagnation point of the vortex pair. The subsaturation is mainly caused by adiabatic compression of the air in the downwelling vortices; the ambient humidity profile is of minor importance. The adiabatic compression leads to an increasing temperature in the vortices, hence to increasing saturation vapor pressure. Since the amount of water in the vortex system is rather decreasing than constant (detrainment), a saturation deficit results. The superimposed velocity field demonstrates that subsaturated air is transported upward along the outer rim of the vortex pair. Although an upward motion is accompanied by adiabatic cooling, this does not compensate for the adiabatic heating before due to the net downward migration of the whole vortex system. Subsaturated air is therefore accumulated around the upper stagnation point of the vortex pair, and part of it is detrained into the region of the secondary wake. It is obvious that the accumulation of subsaturated air around the upper stagnation point dries up the "connection" between the vortex pair and the secondary wake until there opens a vertical wake-gap between these two parts of a young contrail. The IWC at 66 s ST is more than 30 times larger in the vortex cores than in the region between vortices and secondary wake. Also, the IWC in the secondary wake is 10 times larger than in the intermediate region. The detrained subsaturated air leads to a butterfly shape with two IWC maxima in the secondary wake, which is a

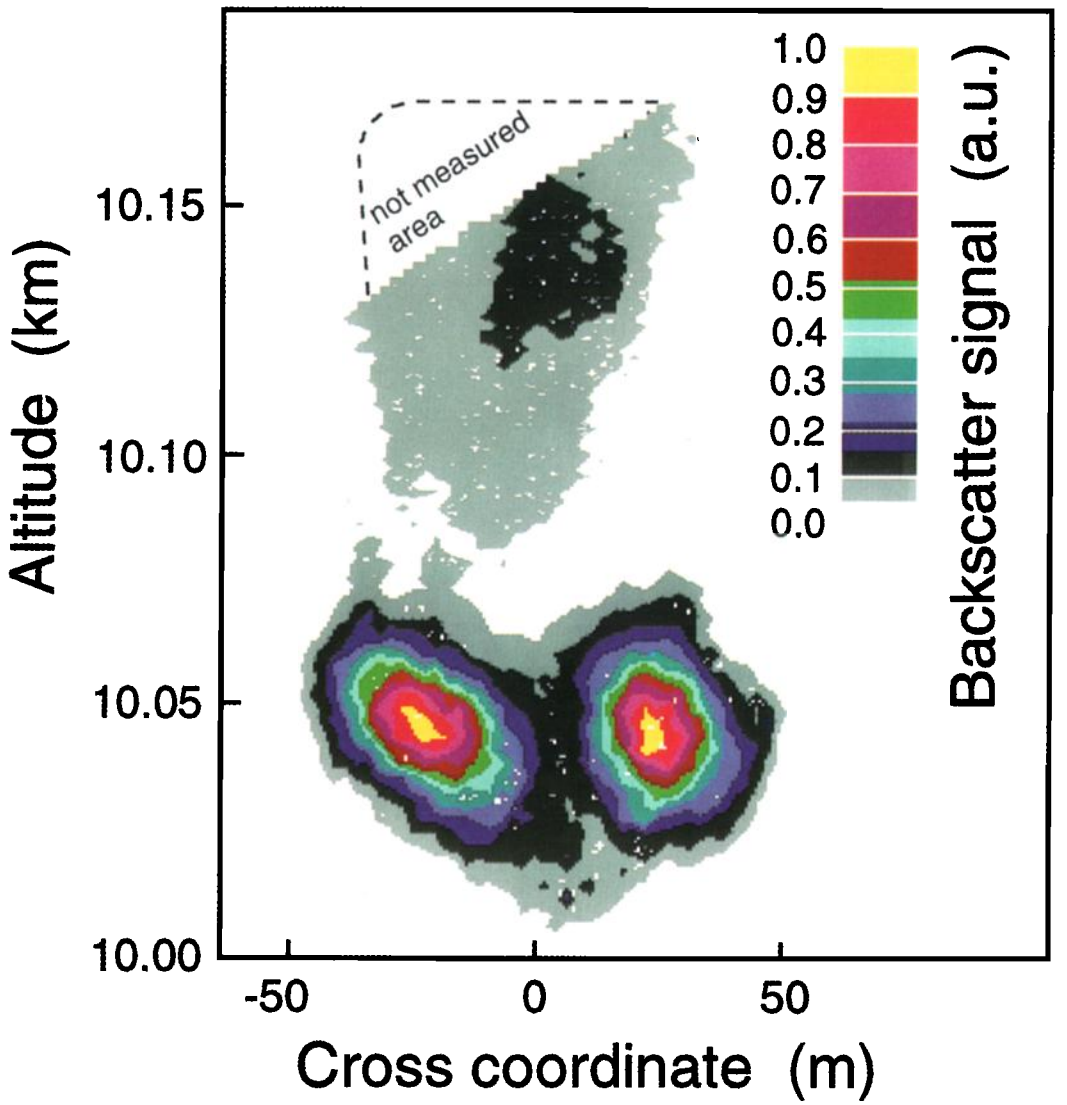

Plate 1. Lidar-derived cross section of the backscatter signal of the contrail of a B-747-400 in the vortex regime showing a secondary wake and the vertical wake-gap phenomenon. The image represents the vertical contrail evolution approximately 50 s behind aircraft. The cross-sectional areas at the moment shown are 4620 and 4410 m^2 for the primary wake and the secondary wake, respectively, where a threshold backscatter signal of 0.1 was used to define the boundary of the contrail.

phenomenon that is seldom observed. It is conjectured that the combined action of wind shear as well as atmospheric and aircraft-induced turbulence usually smears out this pattern, resulting in an IWC field with only one maximum, as observed in most cases (Plate 1).

3.2.2. Microphysical properties. The microphysical properties of the two parts of the young contrail are different. At 72 s ST, when the vertical wake-gap appears in the simulation, the ice masses within the vortices and the secondary wake are similar, 0.88 and 0.81 g/m, respectively. However, there are about 10 times more crystals in the vortices (1.1×10^{12}/m) than in the secondary wake (1.2×10^{11}/m). Accordingly, the ice crystals in the secondary wake have about 10 times more mass than those in the vortex tubes. This also implies that the particles in the secondary wake have more than twice the size than those in the vortices.

This is consistent with the distribution of the linear depolarization ratio measured with the lidar, namely values around 0.5 in the upper part of the contrail, indicating large or nonspherical crystals, and smaller values in the lower part, which indicates small or nearly spherical crystals (section 2.2). The lidar backscatter intensity is (for the small crystals that we are dealing with) about proportional to the ice water path and inversely proportional to the effective radius of the crystal population, i.e., proportional to the local mass extinction coefficient [*Ebert and Curry*, 1992]. Maximum IWC is 1.53 mg/m^3 in the vortex system and 0.67 mg/m^3 in the secondary wake. Together with the size ratio of about $10^{1/3}$ we find a ratio of backscatter intensities of about 5:1 between primary wake and secondary wake, which is consistent with the lidar measurements.

In the further course of time, as the vortices travel farther down, the saturation deficit inside increases more and more. The ice crystals evaporate trying to restore thermodynamic equilibrium (i.e., saturation). However, there is not enough ice for that purpose, so the ice disappears completely. This does

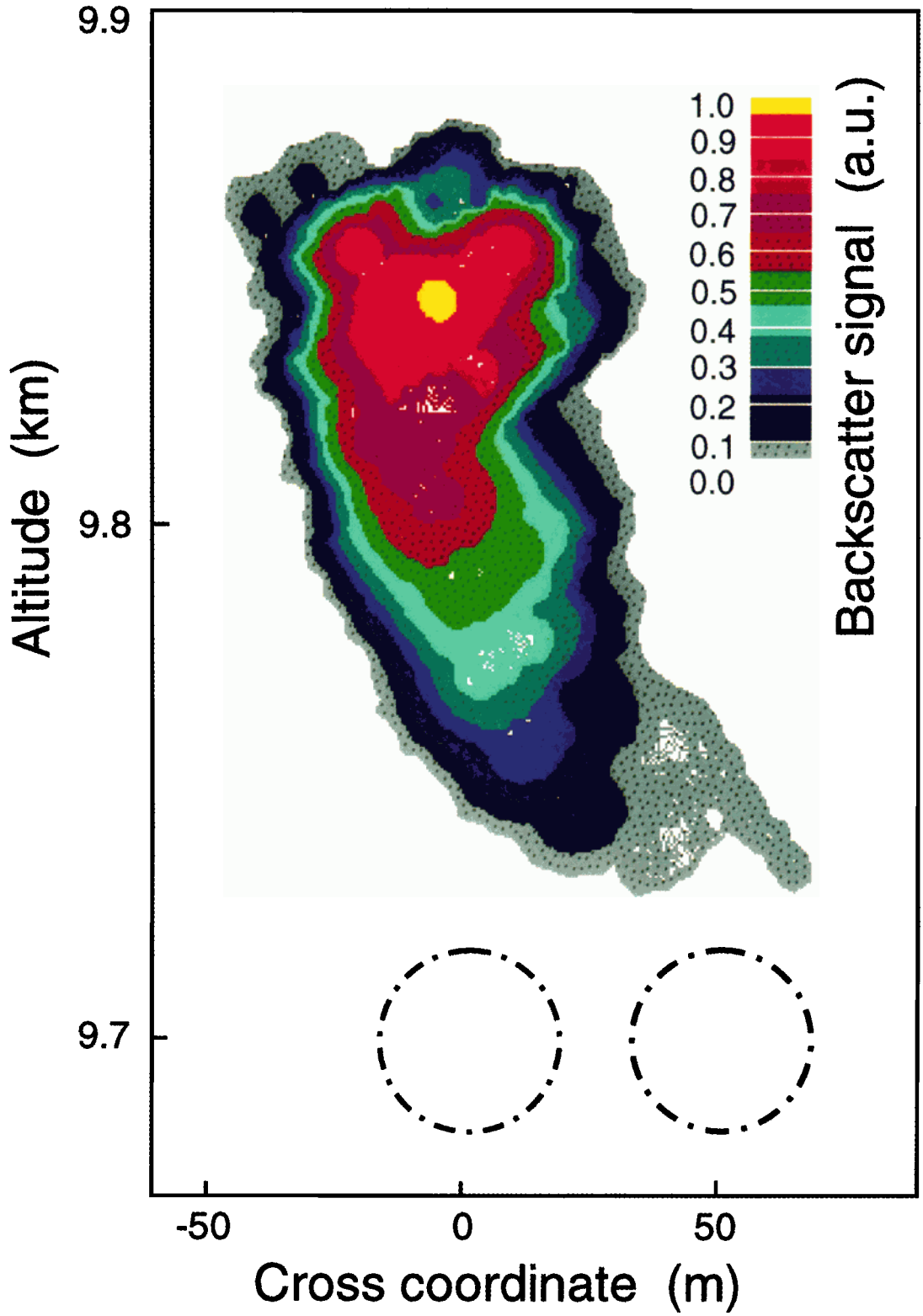

Plate 2. Lidar-derived cross section of the backscatter signal of a contrail in the early dispersion regime at 2.8 min behind aircraft. The ice due to the wingtip vortices in the lower part (dashed circles) has evaporated after vortex breakdown (compare to Plate 1).

not mean that the vortex pair disappears; it is merely no longer marked by the ice crystals. Nonvolatile cores (soot) of the evaporated ice crystals will be further transported down within the vortex tubes until they are released after vortex breakdown (i.e., vortex bursting and/or Crow instabilities [*Crow*, 1970; *Chevalier*, 1973; *Spalart and Wray*, 1996]).

In cases like the one presented here, it is the ice inside the secondary wake that is later considered a persistent contrail.

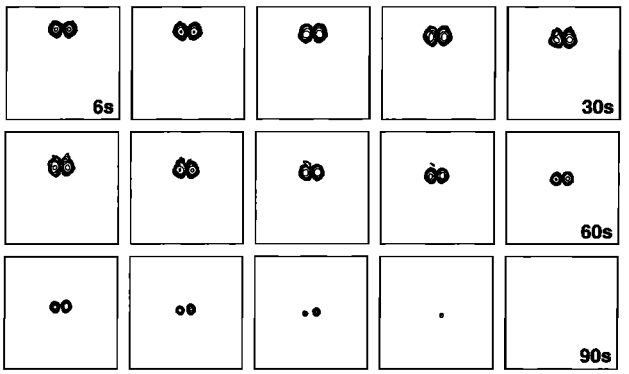

Figure 5. Same as Figure 4 but for scenario 1; that is, the ambient air is subsaturated with respect to ice.

As it was stated in section 2, such cases are relatively frequent, so we must now investigate the properties of the ice in the secondary wake. At 150 s ST behind aircraft there are 1.3 g/m ice in the secondary wake, distributed over 5×10^{10} crystals per meter. Compared to the initial conditions, the ice mass has been reduced by a factor of 10, the number of ice crystals even by a factor of 200. This means that the ice crystals in the wake have, on average, more mass by a factor of 20 than those in the initial plume. The mean mass is 26×10^{-12} g which corresponds to a mean radius of about 2 μm. The ice crystals are distributed over a cross section of 7520 m^2 if a IWC threshold of 0.01 mg/m^3 is used (i.e. the lowest contour in Figures 4–6). The maximum IWC is 0.93 mg/m^3 and the maximum crystal number concentration is 45 cm^{-3}, a value that is still a factor of 10 or more larger than concentrations typical for old contrails or cirrus clouds. The cloud is visible but with a rather faint appearance. The optical depth in the visual wavelength region is less then 0.05. However, since it is located in an ice-supersaturated environment, its ice content will grow further, which will enhance its visibility.

3.3. Sensitivity Studies and Discussion

The results presented above depend on ambient humidity, aircraft weight, exhaust distribution (four or two engines), and other ambient conditions like cross wind and stability. The respective sensitivities are discussed in the following section.

3.3.1. Ambient humidity. First, a case with an ambient humidity of 58% is considered, which means subsaturation with respect to ice in the whole domain. Note that compared to the reference case, the humidity has been reduced by only 2%; however, the effect is striking (Figure 5). There is no secondary wake, and the ice in the vortex system vanishes after 84 s of simulation time (i.e., 105 s plume age). Figure 5 shows that there is sometimes an indication of the secondary wake; however, all the detrained ice is immediately evaporated. Hence a secondary wake cannot form in ice-subsaturated air. This finding is consistent with the empirical description of scenario 1 in section 2. However, there is one difference between the simulation and the observed scenario: in the simulation, the ice in the vortices vanishes gradually by evaporation due to the increasing subsaturation in the descending vortex pair. In the observations the wingtip vortices appear gradually thinner as well (Figure 3). However, at a certain time the wingtip vortices disappear suddenly in the observations due to vortex breakdown (i.e., vortex bursting and/or Crow instabilities [*Crow*, 1970; *Chevalier*, 1973; *Spalart and Wray*, 1996]). Since the model is two-dimensional, these 3-D effects cannot be simulated. This explains the difference between simulation and observation.

An ambient humidity of 65% means ice supersaturation in the whole domain. In this case, ambient humidity is only a few percent higher than in the reference case, but the results are again strikingly different (Figure 6). As in the reference case, there appears a secondary wake right from the beginning of the simulation. The vortex tubes descend, but no vertical wake-gap opens between the descending vortices and the secondary wake. Later in the simulation, the two vortices lose their individuality; that is, only one IWC maximum remains, but this lower part of the contrail does not disappear. This is consistent with the description of scenario 3, as given in section 2. Vortex breakdown is not important in supersaturated environments because as the vortex tubes burst (which cannot be simulated with the present model), the ice crystals are released into the supersaturated air where they find plenty of water vapor to grow on. This is the reason why the Crow instabilities are not easy to see when the air is more than a few percent supersaturated with respect to ice (periodical bulges along the lower edge; see Figure 2). It is interesting to compare the properties of the resulting persistent contrail with those of the persistent secondary wake of the reference case. At the end of the simulation the present contrail has a maximum IWC of 3.39 mg/m^3, and it consists of 26.4 g ice per meter of flight path (which is about a factor of 20 more than in the reference case). The ice is distributed over 5×10^{11} crystals per meter, a factor of 10 more than in the reference case. Accordingly, the mean mass of an ice crystal of 56×10^{-12} g is about twice as large as in the reference case. The maximum crystal number concentration is 190 cm^{-3}. The cloud has a maximum optical depth of 0.4 and is clearly visible. Also here, the humidity in the vortex is below saturation, and the number of ice crystals is about 1/20 of the initial number since many crystals have evaporated during the vortex regime. On the other hand, the ice mass is increasing and will grow on after the end of the vortex regime.

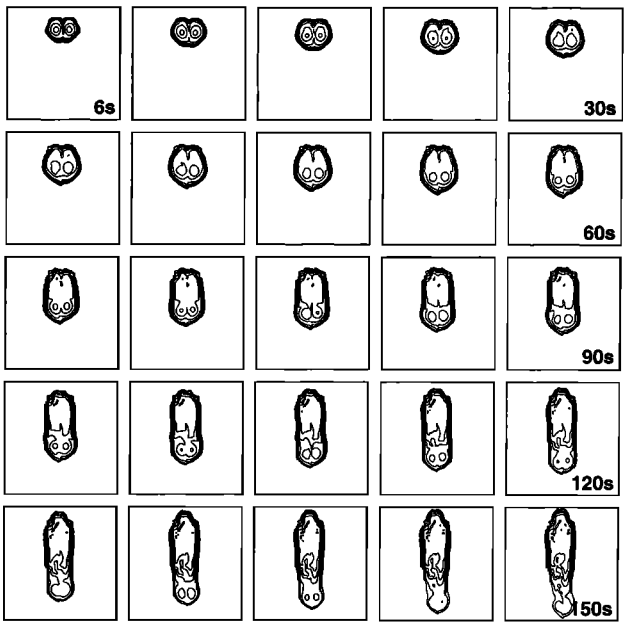

Figure 6. Same as Figure 4 but for scenario 3; that is, the ambient humidity exceeds ice saturation by a few percent.

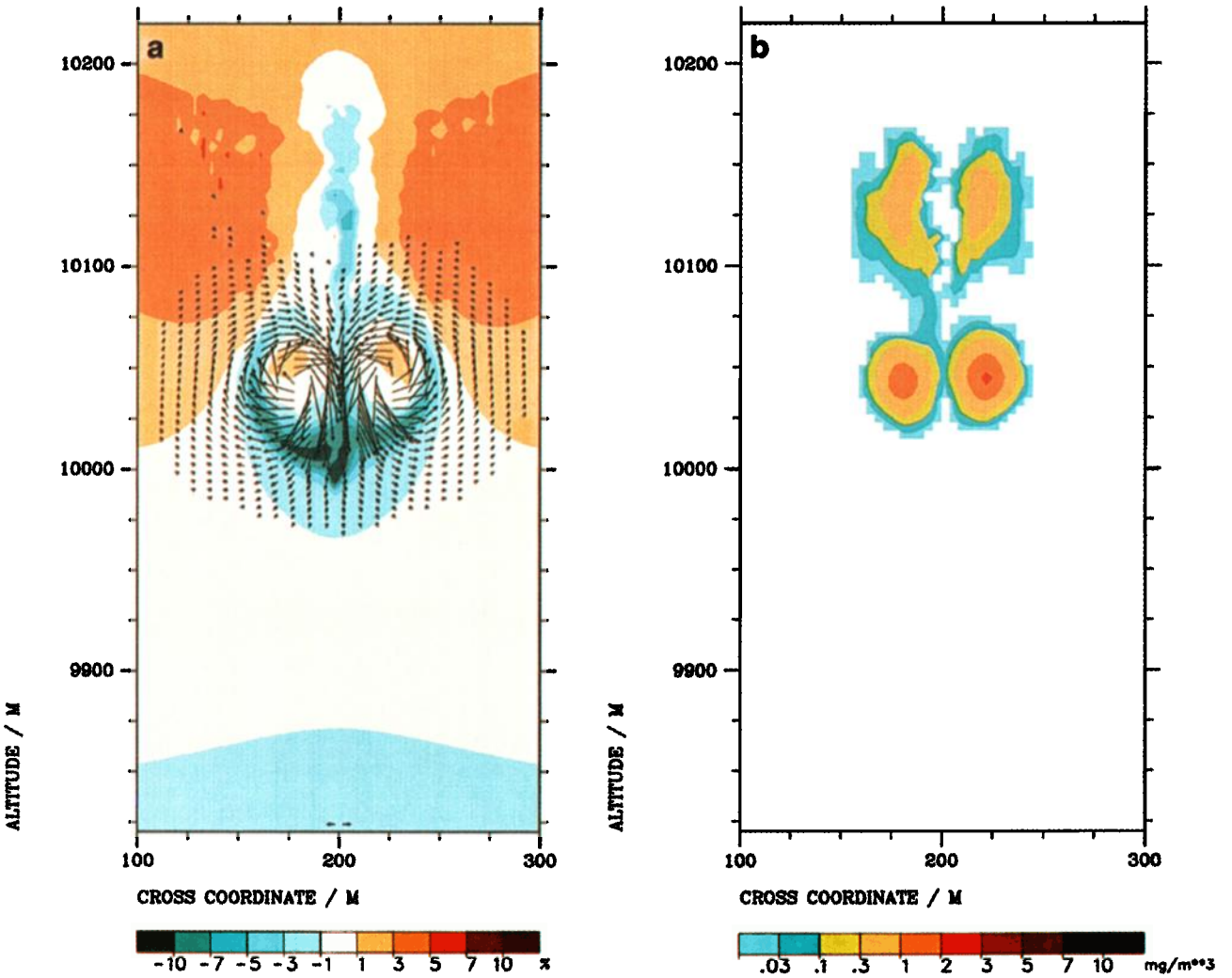

Plate 3. (a) Subsaturation (blue) and supersaturation (red) with respect to ice and velocity field (arrows) in the simulated reference contrail case at a simulation time of 66 s. The air inside the downwelling vortex tubes is subsaturated, which later leads to the complete evaporation of the ice crystals in the vortices. Subsaturated air is transported by the swirling vortex motion around the vortex tubes toward the upper stagnation point where it accumulates and evaporates the ice crystals there. This causes the opening of the vertical wake-gap. (b) Ice water content at 66 s simulation time as in Plate 3a. The cross-sectional areas at the moment shown are 3536 and 5984 m^2 for the primary wake and the secondary wake, respectively, where a threshold IWC of 0.01 mg/m^3 was used to define the boundary of the contrail.

3.3.2. Type of aircraft. The lidar and observational studies indicate that the phenomenon of the vertical wake-gap opening between the descending wingtip vortices and the secondary wake is strongly restricted to big aircraft with four engines. There are two possible explanations for this.

First, the lower amount and differing distribution of exhaust products in the initial plume of a two-engined aircraft leads to different distributions of the ice crystals in the vortex regime. This possibility has been tested by "switching off the outboard engines" in a case that is in all other respects identical to the reference case. (As it has been described in section 3.1 above, the exhaust of the outboard engines has been added by ourselves in an ad hoc way to the concentration field provided by Garnier; so it was easy to switch off the outboard engines). In this case, only 0.5×10^{13} crystals per meter are in the plume initially with a maximum crystal number concentration of less than 5000 cm^{-3}. The initial masses of ice and water vapor (at 60% relative humidity) are 7.5 and 130 g/m, respectively. As in the reference case, only the secondary wake survives the vortex regime of the contrail. A vertical wake-gap appears for the same reason as before in the reference case (at 60 s simulation time), however, at the same time the wingtip vortices vanish due to evaporation of the ice crystals therein. Hence it is certainly difficult to observe a vertical wake-gap in this case. The vortices disappear from sight very early in this simulation because the ice from the outboard engines is missing, which when present is much more concentrated around the vortex cores than the ice from the inboard engines. It can be conjectured that in a case where only the outboard engines are switched on, the secondary wake will be very weak and the ice in the vortex tubes will disappear later (i.e., at 90 s simulation time like in the reference case).

The second possible reason for the absence of a vertical wake-gap in the contrails of two-engined aircraft is the smaller

weight of this kind of aircraft. The circulation of the vortex pair and the downward speed of the vortex system are both proportional to the weight of the aircraft. It is conceivable that the vortex system behind a two-engined aircraft travels downward too slowly for a vertical wake-gap to open before vortex breakdown occurs. The slower downward speed also leads to less subsaturation compared with a four-engined aircraft, and in addition, the slower circulation transports less subsaturated air upward.

The weight of an aircraft changes by a considerable amount during a flight due to fuel use (by ~40% for a B-747). The resulting change of the properties of the vortex system affects the appearance of the secondary wake and the vertical wake-gap. A simulation with all initial velocity vectors reduced by a factor of 0.8 (which means an aircraft weight of 228.3 t), but otherwise identical to the reference case, yields a vertical wake-gap at 90 s simulation time, i.e., around 20 s later than in the reference case. Also, the ice in the vortex system vanishes later than in the reference case, namely at 120 s instead of 96 s. Since the assumed aircraft weight in this case is still much more than the typical weight of two-engined aircraft (say 100 t), it is clear that a vertical wake-gap would open much too late in the wake of such a light aircraft and therefore cannot be observed.

3.3.3. Stratification and shear. Finally, a simulation with the temperature and wind profiles that were measured onboard the FALCON on April 22, 1996, has been performed. Around flight altitude the cross winds (in a reference system that is comoving with the contrail) are relatively slow (typically ± 1 m/s) compared to the swirling velocities in the vortices. Thus the effect of the cross winds on the resulting appearance of the secondary wake is only weak. The measured temperature profile shows a high variability at flight altitude with stable and unstable layers quickly following each other. This has, however, no essential effect on the results; that is, there is no qualitative difference between this case and the more idealistic reference case. It can be conjectured that atmospheric stability has only a weak influence on the appearance of a vertical wake-gap unless the stability is rather high, with a lapse rate of less than about 4.5 K/km. (Lapse rates of this value are probably seldom in the upper troposphere). The downward traveling vortex pair comes to rest in a stably stratified atmosphere after one quarter of the Brunt-Väisällä-period. If this would occur within the vortex regime (i.e., within about 100 s plume age), a strong influence of atmospheric stability on the detachment between the vortex system and the secondary wake should be expected. This would, however, require Brunt-Väisällä-periods of less than 400 s (which is equivalent to a lapse rate of 4.5 K/km), whereas in our simulations a typical value for the period is 11 min. Thus we do not expect an influence of atmospheric stability on the qualitative features of our simulations, namely the appearance of the vertical wake-gap and the later disappearance of the vortices. Indeed, we did not find essential differences between the reference case and the "realistic" case, and no principally new features appear in the latter case.

4. Summary and Conclusions

In the present paper we have investigated the interplay between vortex dynamics and cloud microphysics in young contrails during the vortex regime. By combining lidar cross-section measurements and observational analysis of contrails with numerical simulations of fluid dynamics and microphysics, we were able to show that (1) a secondary wake is only formed in ice-supersaturated air, (2) the secondary wake is the only persistent part of a contrail in the frequent cases with only small ice supersaturation, because the ice in the vortex tubes evaporates due to adiabatic heating as the vortex system travels down, and (3) only in the rare cases of higher ice supersaturation both parts of a contrail (i.e., primary wake and secondary wake) contribute to the persistent ice cloud. Furthermore, we have given an explanation for the vertical wake-gap that often opens between the pair of wingtip vortices and the secondary wake. The vertical wake-gap is produced when subsaturated air is transported upward along the outer edges of the sinking vortex tubes and accumulates around the upper stagnation point of the vortex system. Any ice present near the stagnation point then evaporates, leaving a gap in the IWC field.

We conclude from these findings that contrail evolution strongly depends on the type of aircraft. The vertical wake-gap occurs preferably in wakes of heavy (four engined) aircraft. In the wakes of light two-engined aircraft the vortices migrate down too slowly, so the opening of the vertical wake-gap would not occur before the end of the vortex regime.

From the observational analysis of contrails we found that the frequency distribution of RH_i in the tropopause region shows a maximum at and slightly above 100%. The preference of the humidity for a value close to ice saturation (at least in case contrails are present) may be a general feature of the upper troposphere but may also be a result of the orographic influence of the Alps. The search for physical mechanisms that lead to the inferred humidity distribution seems to be a challenging task.

According to our results the number of ice crystals that survive the vortex regime is relatively small compared to the number of ice crystals present in the early jet regime of a contrail. How large the surviving fraction of ice crystals is depends strongly on ambient humidity. In the most frequent reference case where only the secondary wake is persistent ($RH_w = 60\%$), the surviving fraction is 1/200, whereas in the moister case with $RH_w = 65\%$ (where also ice in the vortex tubes reaches the end of the vortex regime), the surviving fraction is 1/20. In reality, these fractions may be larger because coatings of foreign material on the ice crystals may delay their evaporation. However, in the model we assumed pure ice. Anyway, there is no possibility to infer the emission index of particles from a measured number of ice crystals in an older contrail. The evaporating crystals leave back the nonvolatile nucleus where they were formed on initially. From these results we predict that large numbers of nonvolatile (soot) particles should be present at about 100 m beneath persistent contrails in situations that lead to scenario 2. In contrails that pertain to scenario 3 the number of interstitial particles should increase toward their bottom edge. Measurements of these particles are strongly recommended.

Finally, we give some hint how to minimize the formation of persistent contrails by technical means. We found that for heavy aircraft all the ice that is not detrained from the wingtip vortices is brought downward and evaporates eventually; and vice versa, only the part that has been detrained evolves into a persistent ice cloud in most cases. From this we conclude that the use of heavy aircraft and minimizing detrainment is a means of minimizing persistent contrails. Technical possibilities to minimize detrainment could be an optimized position of the engines (preferably shifted toward the wing tips, leading to

a trade-off against other problems, of course). Also, the construction of wings might by optimized in order to achieve a distribution of the wing loading that minimizes detrainment.

Acknowledgments. The authors would like to thank F. Garnier (ONERA) and D. Taleb (U. Strasbourg) for providing data for initializing the model as well as E. Jensen (NASA) for providing the microphysics code. They are indebted to T. Gerz and F. Schröder (DLR) for valuable discussions. The careful reading of the manuscript by W. R. Stockwell (IFU) is gratefully acknowledged. This research has been supported by the German Bundesministerium für Bildung, Wissenschaft, Forschung und Technologie within the joint project "Schadstoffe in der Luftfahrt (Pollutants from Air Traffic)" and by the Comission of the European Union within "AEROCONTRAIL" of the Environment and Climate Program.

References

Anderson, B. E., W. R. Cofer, D. R. Bagwell, J. W. Barrick, C. H. Hudgins, and K. E. Brunke, Airborne observations of aircraft aerosol emissions, I, Total and nonvolatile particle emission indices, *Geophys. Res. Lett.*, *25*, 1689–1692, 1998.

Appleman, H., The formation of exhaust condensation trails by jet aircraft, *Bull. Am. Meteorol. Soc.*, *34*, 14–20, 1953.

Chevalier, H., Flight test studies of the formation and dissipation of trailing vortices, *J. Aircraft*, *10*, 14–18, 1973.

Chlond, A., Large-eddy simulations of contrails, *J. Atmos. Sci.*, *55*, 796–819, 1998.

Crow, S. C., Stability theory for a pair of trailing vortices, *AIAA J.*, *8*, 2172–2179, 1970.

DeMott, P. J., M. P. Meyers, and W. R. Cotton, Parameterization and impact of ice initiation processes to numerical model simulations of cirrus clouds, *J. Atmos. Sci.*, *51*, 77–90, 1994.

Dürbeck, T., and T. Gerz, The dispersion of aircraft exhausts in the free atmosphere, *J. Geophys. Res.*, *101*, 26,007–26,015, 1996.

Ebert, E. E., and J. A. Curry, A parameterization of ice cloud optical properties for climate models, *J. Geophys. Res.*, *97*, 3831–3836, 1992.

Freudenthaler, V., F. Homburg, and H. Jager, Contrail observations by ground-based scanning lidar: Cross-sectional growth, *Geophys. Res. Lett.*, *22*, 3501–3504, 1995.

Garnier, F., S. Brunet, and L. Jacquin, Modelling exhaust plume mixing in the near field of an aircraft, *Ann. Geophys.*, *15*, 1468–1477, 1997.

Gerz, T., and T. Ehret, Wake dynamics and exhaust distribution behind cruising aircraft, in *The Characterization and Modification of Wakes From Lifting Vehicles in Fluids*, *AGARD Conf. Proc.*, *584*, 35.1–35.8, 1996.

Gerz, T., and T. Ehret, Wingtip vortices and exhaust jets during the jet regime of aircraft wakes, *Aerosp. Sci. Technol.*, *7*, 463–474, 1997.

Gierens, K. M., Numerical simulations of persistent contrails, *J. Atmos. Sci.*, *53*, 3333–3348, 1996.

Gierens, K. M., and J. Ström, A numerical study of aircraft wake induced ice cloud formation, *J. Atmos. Sci.*, *55*, 3253–3263, 1998.

Jensen, E. J., O. B. Toon, D. L. Westphal, S. Kinne, and A. J. Heymsfield, Microphysical modeling of cirrus, 1, Comparison with 1986 FIRE IFO measurements, *J. Geophys. Res.*, *99*, 10,421–10,442, 1994.

Kärcher B., R. Busen, A. Petzold, F. P. Schröder, U. Schumann, and E. J. Jensen, Physicochemistry of aircraft-generated liquid aerosols, soot, and ice particles, II, Comparison with observations and sensitivity studies, *J. Geophys. Res.*, *103*, 17,129–17,147, 1998.

Miake-Lye, R. C., M. Martinez-Sanchez, R. C. Brown, and C. E. Kolb, Plume and wake dynamics, mixing, and chemistry behind a high-speed civil transport aircraft, *J. Aircraft*, *30*, 467–479, 1993.

Petzold, A., et al., Near-field measurements on contrail properties from fuels with different sulfur content, *J. Geophys. Res.*, *102*, 29,867–29,880, 1997.

Ponater, M., S. Brinkop, R. Sausen, and U. Schumann, Simulating the global atmospheric response to aircraft water vapour emissions and contrails: A first approach using a GCM, *Ann. Geophys.*, *14*, 941–960, 1996.

Pruppacher, H. R., and J. D. Klett (Eds.), *Microphysics and Precipitation*, 2nd ed., 438 pp., Kluwer Acad., Norwell, Mass., 1997.

Quackenbush, T. R., M. E. Teske, and A. J. Bilanin, Computation of wake/exhaust mixing downstream of advanced transport aircraft, *AIAA J.*, *93-2944*, 15, 1993.

Sassen, K., Contrail-cirrus and their potential for regional climate change, *Bull. Am. Meteorol. Soc.*, *78*, 1885–1902, 1997.

Schilling, V., S. Siano, and D. Etling, Dispersion of aircraft emissions due to wake vortices in stratified shear flows: A two-dimensional numerical study, *J. Geophys. Res.*, *101*, 20,965–20,974, 1996.

Schumann, U., On conditions for contrail formation from aircraft exhausts, *Meteorol. Z.*, *5*, 4–23, 1996.

Schumann, U., T. Hauf, H. Höller, H. Schmidt, and H. Volhert, A mesoscale model for simulation of turbulence, clouds, and flow over mountains: Formulation and validation examples, *Beitr. Phys. Atmos.*, *60*, 413–446, 1987.

Scorer, R. S., and L. J. Davenport, Contrails and aircraft downwash, *J. Fluid Mech.*, *43*, 451–464, 1970.

Spalart, P. R., On the motion of laminar wing wakes in a stratified fluid, *J. Fluid. Mech.*, *327*, 139–160, 1997.

Spalart, P. R., and A. A. Wray, Initiation of the crow instability by atmospheric turbulence, in *The Characterization and Modification of Wakes From Lifting Vehicles in Fluids*, *AGARD Conf. Proc.*, *584*, pap. 18, 1996.

Sussmann, R., Optical properties of contrail-induced cirrus: Discussion of unusual halo phenomena, *Appl. Opt.*, *36*, 4195–4201, 1997.

Sussmann, R., Vertical dispersion of an aircraft wake: Aerosol-lidar analysis of entrainment and detrainment in the vortex regime, *J. Geophys. Res.*, this issue.

K. M. Gierens, DLR, Institut für Physik der Atmosphäre, Postfach 1116, D-82230 Wessling, Germany. (klaus.gierens@dlr.de)

R. Sussmann, Fraunhofer-Institut für Atmosphärische Umweltforschung, Kreuzeckbahnstrasse 19, D-82467 Garmisch-Partenkirchen, Germany. (sussmann@ifu.fhg.de)

(Received May 21, 1998; revised August 27, 1998;
accepted September 1, 1998.)